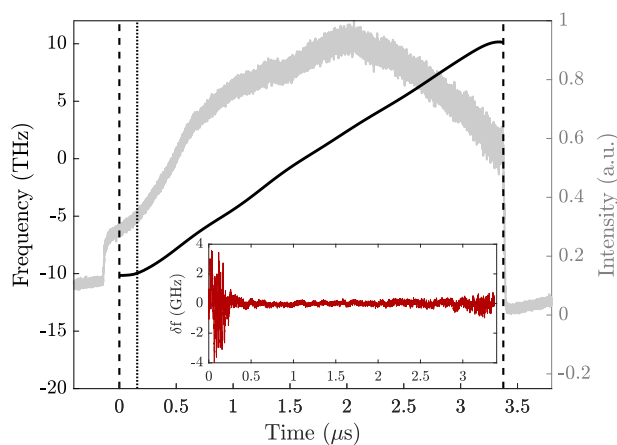


# Real-Time Experimental Measurement of Swept Source VCSEL Properties Relevant to OCT Imaging

Volume 9, Number 5, October 2017

T. P. Butler  
S. Slepneva  
P. M. McNamara  
K. Neuhaus  
D. Goulding  
M. Leahy  
G. Huyet



DOI: 10.1109/JPHOT.2017.2752644

1943-0655 © 2017 IEEE

# Real-Time Experimental Measurement of Swept Source VCSEL Properties Relevant to OCT Imaging

T. P. Butler,<sup>1,2,3</sup> S. Slepneva,<sup>1,2</sup> P. M. McNamara,<sup>4</sup> K. Neuhaus,<sup>3</sup>  
D. Goulding,<sup>1,2</sup> M. Leahy,<sup>4</sup> and G. Huyet<sup>1,2,5,6</sup>

<sup>1</sup>Centre for Advanced Photonics and Process Analysis, Cork Institute of Technology, Cork T12 P928, Ireland

<sup>2</sup>Tyndall National Institute, University College Cork, Cork T12 R5CP, Ireland

<sup>3</sup>Max Planck Institute of Quantum Optics, Garching 85748, Germany

<sup>4</sup>School of Physics, National University of Ireland Galway, Galway H91 TK33, Ireland

<sup>5</sup>Université Côte d'Azur, CNRS, Institut de Physique de Nice, Valbonne F-06560, France

<sup>6</sup>National Research University of Information Technologies, Mechanics and Optics, Saint Petersburg 197101, Russia

DOI:10.1109/JPHOT.2017.2752644

1943-0655 © 2017 IEEE. Translations and content mining are permitted for academic research only.

Personal use is also permitted, but republication/redistribution requires IEEE permission.

See [http://www.ieee.org/publications\\_standards/publications/rights/index.html](http://www.ieee.org/publications_standards/publications/rights/index.html) for more information.

Manuscript received May 16, 2017; revised September 5, 2017; accepted September 11, 2017. Date of publication September 14, 2017; date of current version October 6, 2017. The work was supported in part by the Science Foundation Ireland under Contract 11/PI/1152 and IPIC (12/RC/2276), in part by NUI Galway, Galway University Foundation, the University of Limerick Foundation, the National Biophotonics Imaging Platform (NBIP) Ireland funded under the Higher Education Authority PRTL Cycle 4, co-funded by the Irish Government and the European Union - Investing in your future, and Compact Imaging, Inc. Corresponding author: Thomas Butler (e-mail: thomas.butler23@gmail.com).

**Abstract:** A real-time study of the dynamic properties of a frequency swept vertical cavity surface emitting laser (VCSEL) is presented. Such tunable laser sources have previously been shown to provide long coherence lengths and improved performance in metrology and imaging applications. Single-shot interferometric reconstruction of both the phase and intensity of the swept source allows for experimental measurement of the full complex electric field over multiple sweep periods. Access to the electric field enables direct measurement of laser properties that can be related to the imaging performance of the laser when used in a swept source optical coherence tomography application. Both inter-sweep and intra-sweep characterization is possible, including determination of the instantaneous spectral shape, sweep rate, linewidth, coherence roll-off, and point spread function.

**Index Terms:** Semiconductor lasers, optical coherence tomography (OCT).

## 1. Introduction

Optical coherence tomography (OCT) is an imaging technique that allows for the creation of high resolution, 3-dimensional volumetric images in semi-transparent scattering media [1]. Typically imaging depths of several millimetres to centimetres are achievable in biological tissues, with an axial resolution of tens of microns [2]. With rapid image acquisition techniques, 3D tomography volumes can be imaged in real-time. This unique combination of capabilities of the OCT imaging modality places it in an ideal position to bridge the gap between microscopic imaging techniques and macroscopic imaging (for example ultrasound imaging). Furthermore, fully 3-dimensional imaging of a sample makes this technique ideal for non-invasive imaging studies and in-vivo applications.

The range of applications of the technique has grown steadily since its inception, with areas such as retinal imaging [3], dental imaging [4], respiratory medicine [5] and endoscopic imaging [6] now utilising OCT techniques. Outside of the medical imaging sector, OCT is being investigated as a tool for industrial sensing of devices and surfaces, especially in areas such as production line non-destructive testing (NDT) [7].

Swept source optical coherence tomography (SS-OCT) has emerged in the last decade as the leading technique for the acquisition of images with a high sensitivity and fast imaging rate [8]. The key enabling technology in this method lies in the frequency tunable light source used as the imaging probe. This light source produces a periodic variation in the output wavelength, which changes the output wavelength over a large bandwidth while remaining spectrally narrow over any short time period. By frequency modulating the probing light in such a manner it is possible to perform a spectral interferometry measurement in order to reconstruct the reflectivity profile of the desired sample, for example biological tissue. With spectral discrimination of the light performed in the temporal domain only a single detector is required, while the imaging rate is determined by the repetition rate of the wavelength sweep. In this configuration, single axial scan imaging rates ranging from several hundred kilohertz up to Megahertz are possible.

Several laser configurations have been developed and applied to SS-OCT imaging, including Fourier domain mode-locked lasers (FDMLs) [9], external cavity lasers [10], sampled-grating distributed Bragg reflector lasers [11], and micro electro-mechanical systems (MEMs) based lasers [12]. A recently developed MEMs based laser has been demonstrated based on a tunable vertical cavity surface emitting laser (VCSEL) cavity [13]. This laser has been shown to offer superior imaging depths compared to similar technologies [14].

VCSEL devices are suited to imaging applications for a number of reasons. By incorporating the top dielectric mirror of the device with a MEMs based actuator the cavity length of the device, and thus the emission wavelength, can be rapidly varied. A VCSEL micro-cavity can be engineered to only support a single cavity mode within the bandwidth of the gain region, ensuring highly coherent single wavelength emission across a bandwidth of 100 nm or more [15], [16]. These three properties (wide bandwidth, high coherence, and fast tuning) are important elements in the formation of high resolution, real-time volumetric images.

While several techniques exist for the characterisation of swept sources and SS-OCT apparatus, a complete time-resolved study of swept sources has been, until recently, unavailable. Previous studies that have attempted to perform an analysis of the properties of swept frequency lasers were limited to either multi-shot [17] or multi-sweep [18] averaging techniques. Such time-averaging techniques remove the ability to characterise different parts of the wavelength sweep simultaneously, as well as characterising the changing properties of consecutive sweeps. Recently, a novel interferometric technique which can perform a real-time, single-shot reconstruction of the complex electric field of a swept laser [19] has been demonstrated. Using this technique, the temporal and spectral properties of a short cavity laser were examined, including a measurement of the instantaneous linewidth and coherence roll-off. In this work, the technique is applied to study, for the first time, the instantaneous characteristics of a frequency swept VCSEL. The analysis is further expanded to consider multiple laser properties that have a direct bearing on the imaging performance, highlighting the expected strengths and weaknesses of the source when applied to OCT imaging.

## 2. Experimental Set-Up

The device used in this work was a commercially available swept source VCSEL developed by Thorlabs Inc. [20]. Fig. 1 illustrates the internal components of the light source. The MEMs based tunable VCSEL is optically pumped, with the chip output monitored using an internal photodiode. A booster semiconductor optical amplifier (SOA) is used in order to amplify and shape the output intensity. Finally, a k-clocking Mach-Zehnder interferometer samples part of the output field in order to produce a temporal clock that can be used to sample the imaging field in equal frequency steps.

The output of the swept source is directed into a branching characterisation apparatus which measures the spectrum, intensity, and phase. The phase measurement interferometer utilises a

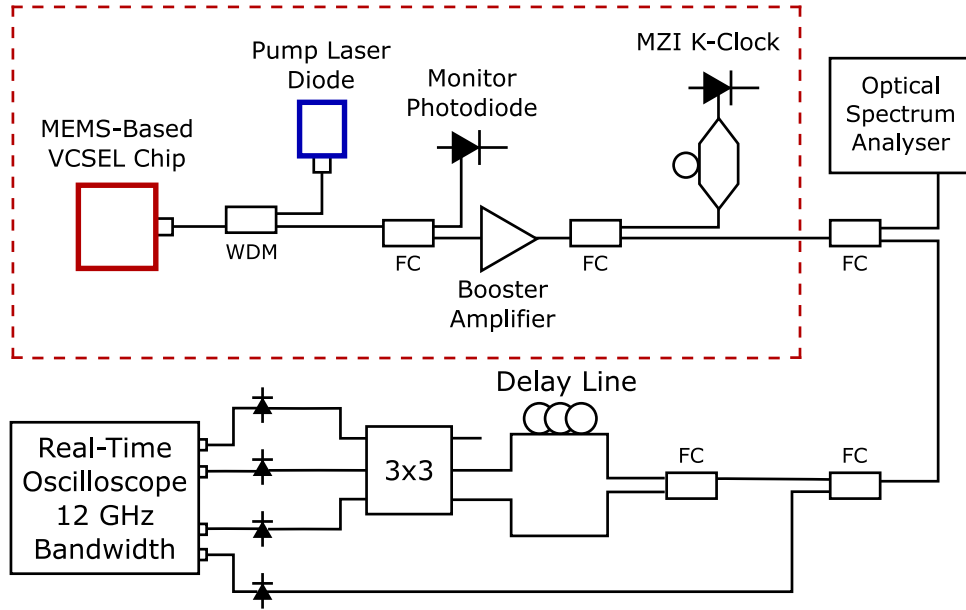


Fig. 1. Experimental setup of the electric field reconstruction technique applied to the swept source VCSEL. FC - fibre coupler, WDM - wavelength division multiplexer.

self-delayed heterodyne detection technique, which has been previously used to measure the time-resolved phase dynamics of semiconductor lasers and swept sources [21]. A fibre coupler is used to create two optical paths, with a small fibre delay inserted into one arm. The laser field is then mixed with the delayed signal using a  $3 \times 3$  fiber coupler with a  $120^\circ$  phase delay. The output electric field of each port is a summation of the three input port signals, with a phase delay added to 2 of the ports. For example, the output of port one is given by:

$$E_1^o = \frac{1}{\sqrt{3}} \left( A_1 e^{i\phi_1} + A_2 e^{i(\phi_2 + \frac{2\pi}{3})} + A_3 e^{i(\phi_3 + \frac{2\pi}{3})} \right), \quad (1)$$

where  $A_n$  is the amplitude of the field at port  $n = 1, 2, 3$ , and  $\phi_n$  is the corresponding field phase. With only two input fields, the output intensities can be combined to measure the phase difference between the input signals,  $\eta$ . The phase difference is calculated from

$$\eta(t) = \arctan \left( \frac{\sqrt{3}}{2} \frac{I_1 - I_2}{I_3 - \frac{1}{2}(I_1 + I_2)} \right), \quad (2)$$

where  $I_n = |E_n^o|^2$ , the intensity measured at the output of each port.

In this experiment, the phase difference  $\eta(t)$ , will take the form,

$$\eta(t) = \phi(t) - \phi(t - \tau), \quad (3)$$

where  $\phi$  is the original phase of the laser field and  $\tau$  is the short time delay introduced in the interferometer arms ( $\tau = 1.1$  ns for reconstruction of the VCSEL laser). It is possible to express the original phase of the laser as a function of  $\eta(t)$  via a Taylor series expansion around the point  $t - \tau$ ,

$$\frac{d\phi(t)}{dt} \approx \frac{\eta(t)}{\tau} + \frac{1}{2} \frac{d\eta(t)}{dt}, \quad (4)$$

assuming that the delay  $\tau$  is sufficiently short. The time-resolved instantaneous frequency of the field,  $f(t)$  (or equivalently wavelength,  $\lambda(t)$ ) can be derived from the phase,

$$f(t) = \frac{c}{\lambda(t)} = \frac{1}{2\pi} \frac{d\phi(t)}{dt}, \quad (5)$$

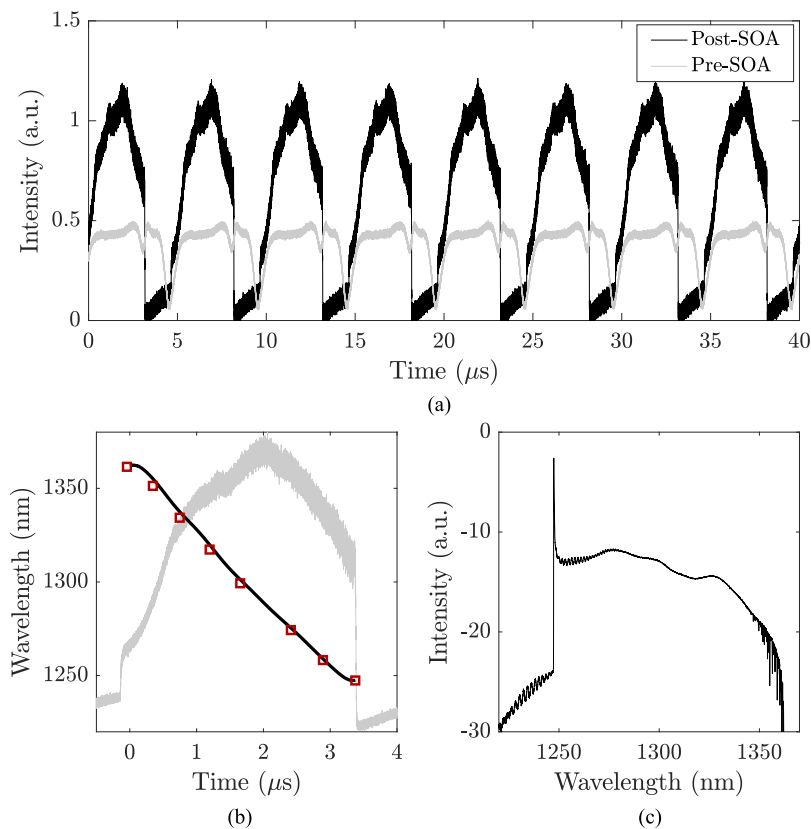


Fig. 2. (a) Time-resolved intensity of the swept VCSEL measured by the internal pre-booster photodiode (grey) and external post-SOA intensity (black). (b) Reconstructed wavelength (line) from the  $3 \times 3$  interferometric method and TLS method (squares), along with the intensity of a single sweep (grey). (c) Average optical spectrum.

where  $c$  is the speed of light.

Simultaneous to the phase measurement, the fourth channel of the real-time oscilloscope is used to record the instantaneous intensity,  $I(t)$ , of the swept source. These two quantities,  $\phi(t)$  and  $I(t)$ , are sufficient to reconstruct the entire complex electric field of the laser in a real-time, single-shot format. Fig. 2 presents an example of the recovered characterisation signals. Fig. 2(a) compares the output intensity of the laser before being amplified by the booster SOA, and the intensity,  $I(t)$ , measured by the high-speed photodiode and oscilloscope. The laser operates with a sweep rate of 200 kHz, and an average output power greater than 20 mW. The indicated intensity time-series are shown with arbitrary scaling for ease of comparison. The SOA amplification process ensures that the intensity is sufficient for OCT applications. The SOA furthermore modulates the intensity, switching off the laser intensity during the unusable section of the sweep. During this time, the laser emission is incoherent, consisting mainly of spontaneous emission noise from the SOA. Low coherence during the “off” region of the sweep means that phase reconstruction of the electric field is impossible. Fig. 2(b) illustrates the recovered instantaneous wavelength corresponding to a single sweep period. This instantaneous wavelength function shows the extent of the phase reconstruction that was possible using the self heterodyne interferometric method. Also shown is an independent verification measurement used to track the wavelength sweep. This measurement is conducted by mixing the swept output of the laser with a single-mode fixed local oscillator. By comparing the time of the beating between the two signals with the wavelength of the local oscillator, the wavelength sweep is mapped and is in excellent agreement with the recovered wavelength sweep from the  $3 \times 3$  technique. The time-resolution of the reconstruction is limited

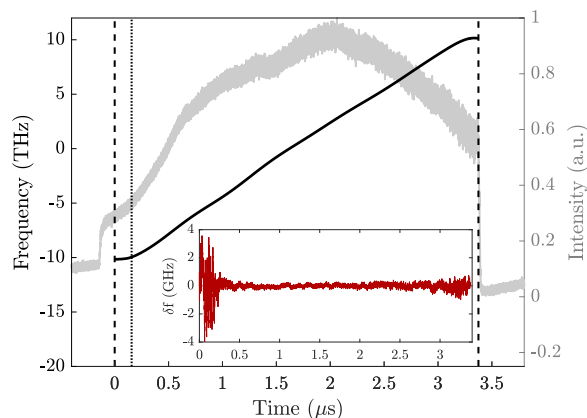


Fig. 3. Reconstructed instantaneous frequency during a single sweep period (black), with the corresponding intensity (grey). Dashed lines indicate the extent of the recoverable frequency data, while the dotted line shows the OCT imaging start trigger time. (Inset) Frequency deviation  $\delta f$  after subtraction of the overall sweep shape.

only by the maximum detection bandwidth of the fast photodiodes (New-focus model 1554-B) and oscilloscope (Agilent DSO91304A). The full temporal period which can be detected is limited by the maximum memory depth of the oscilloscope. In this case, it is possible to record the field at a sampling rate of 40 GSa/s over 39 consecutive sweeps. Finally, Fig. 2(c) shows the time-averaged optical spectrum. The center wavelength is approximately 1303 nm, with a sweep bandwidth of  $\sim 83$  nm. Comparison with the time-averaged spectrum and local oscillator method both verify that the phase reconstruction technique is accurately recovering the correct time-resolved frequency of the sweep. With access to the electric field of the laser, it is now possible to calculate laser properties which can be used to directly infer the imaging performance of the swept laser.

### 3. Experimental Results

In SS-OCT imaging, the coherence of the light source is often responsible for a sensitivity decay with imaging depth [22]. This coherence roll-off effect is more pronounced for light sources with a wider instantaneous spectrum. Time resolved measurement of this spectral width allows for examination of the coherence across a single sweep period. Direct measurement of the laser linewidth is impossible due to the constantly varying central frequency of the laser emission. Previous work on the measurement of the dynamic linewidth has utilised short-time gating of the sweep in order to minimise the effect of the sweep [17]. Fast-gating the output of the laser relies on the assumption that the during the gate, the spectral width is dominated by the linewidth of the laser, and not the changing central frequency. By allowing access to the full electric field during the sweep, the  $3 \times 3$  technique offers an opportunity to numerically remove the deterministic movement of the central frequency,  $\tilde{f}$ , from the measured instantaneous frequency of the field,  $f(t) = d\phi/dt$ . In this case, the remaining stationary noise term,  $\delta f$  describes the average linewidth, and contains contributions from the intrinsic phase-noise of the laser as well as the thermal brownian noise of the MEMs actuated mirror [23]. In order to approximate the deterministic frequency sweep term, an interpolated spline fit is made of the frequency sweep under-sampled at 10 MHz. The residual term is calculated as

$$\delta f = f(t) - \tilde{f} \quad (6)$$

and is plotted in the inset of Fig. 3. The slow sweep fit is chosen such that the remaining frequency noise is a stationary signal with a mean of zero over each measurement period (25 ns). The stationary electric field,  $E_s(t)$ , of the laser can now be reconstructed using the frequency deviation

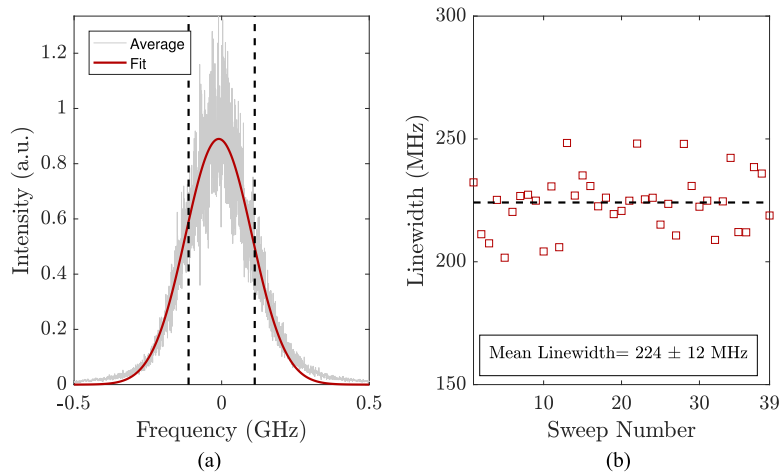


Fig. 4. (a) Average power spectral density of the static (filter-frame) electric field. The PSD is fit with a Gaussian lineshape. The average linewidth of the sweep is indicated by the dashed lines. (b) Average single-sweep linewidth over the course of 39 consecutive sweeps, with an average of 224 MHz.

instead of the swept frequency, according to

$$E_s(t) = \sqrt{I(t)} \exp\left(i2\pi \int_0^t \delta f(t') dt'\right). \quad (7)$$

This new field represents a transform of the electric field into the frame of reference of the sweeping mode. Examining the spectral width of the transformed field yields a measurement of the instantaneous linewidth of the laser in this frame. The power spectral density (PSD),  $S(f)$  is calculated using the fast Fourier transform (FFT) of the field. The spectral width of the lineshape is defined using the concept of the power-equivalent coherence time. This definition of the coherence time of the field is inversely proportional to the spectral width, and can be found via

$$\frac{1}{\tau_c} = \Delta f = \frac{\left(\int_{-\infty}^{+\infty} S(f) df\right)^2}{\int_{-\infty}^{+\infty} S(f)^2 df}, \quad (8)$$

where  $\tau_c$  is the coherence time of the field and  $\Delta f$  the corresponding spectral width.

The PSD is calculated for each of the 39 recorded sweeps, and the average PSD is plotted in Fig. 4(a). The time averaged lineshape is well approximated with a Gaussian function. Fig. 4(b) plots the linewidth across all of the sweeps calculated using (8). The instantaneous linewidth is measured to be  $224 \text{ MHz} \pm 12 \text{ MHz}$ . This linewidth corresponds to a coherence time of  $\sim 4.5 \text{ ns}$ . Compared to other studies of the instantaneous linewidth of swept sources, for example FDML [24] or short cavity lasers [19], this measured value of the linewidth is at least one order of magnitude smaller (12–17 GHz for the FDML and 5–6 GHz for the short cavity). In SS-OCT, the coherence length of the source determines the maximum imaging depth achievable. Clear OCT imaging should be possible over distances on the order of half the coherence length,

$$z_c = \frac{l_c}{2} = \frac{c\tau_c}{2}, \quad (9)$$

where  $l_c$  is the coherence length corresponding to the coherence time defined above,  $z_c$  is the coherence imaging depth, and the factor of 2 accounts for the optical path length of the light in the interferometer arm. This measurement of the VCSEL coherence suggests a coherence imaging depth of 67 cm. OCT imaging systems using VCSEL lasers has previously achieved such large imaging depths [13], [14], as well as with more recent FDML [25] and akinetic systems [26],



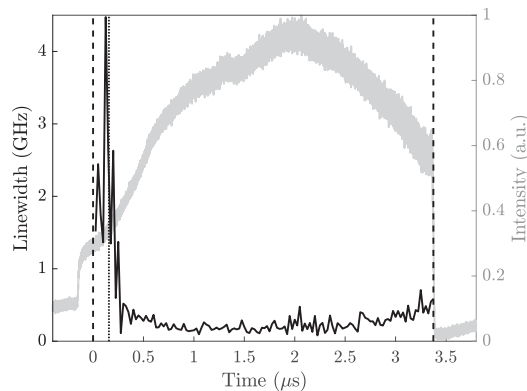


Fig. 5. Time-resolved instantaneous linewidth of the VCSEL over the course of a single sweep. The corresponding intensity is displayed in grey. The dashed lines indicate the extent of the recoverable phase, while the dotted line indicates the clock start signal.

with the most recent demonstration of the VCSEL OCT system achieving cubic meter volume tomography [27].

While the average value of the instantaneous linewidth is useful as a general indicator of laser coherence, a full time-resolved measurement of the linewidth during the sweep is required for complete characterisation of laser performance. Using the electric field reconstruction technique, the dynamic linewidth can be calculated simply by binning the electric field time series and considering the PSD at several points during the sweep. Once again, the  $3 \times 3$  technique has advantages over other multi-shot measurements because it captures each section of the sweep, and indeed multiple sweeps, in a single recording. Fig. 5 displays the calculated instantaneous linewidth of the VCSEL over the course of a single sweep (corresponding to the first sweep shown in Fig. 4(b)). The linewidth is calculated in 25 ns long sections. While the average linewidth was calculated to be above 200 MHz, it is clear that the linewidth is not so high during the entire sweep period. The linewidth during the start of the sweep is considerably higher than later times, at over 1 GHz. This behaviour is somewhat accounted for in the imaging process. The figure shows a dotted line which indicates the clock start trigger time supplied by the device and used for image acquisition. With this in mind, the highest linewidth section of the sweep is generally not included in the imaging signal. This time-resolved analysis also reveals, however, that the linewidth still remains above the average level during the first 250–500 ns after the start of the acquisition. Such a result is useful for future device improvement and optimisation as it provides improved insight for the design of the optimal image acquisition times. Toward the end of the sweep, a rise in the linewidth is also observed. This increasing linewidth is possibly linked to the slowing down of the sweep of the central frequency position of the laser emission. The time-resolved linewidth has also been calculated for the other recorded sweeps. While the average linewidth varies by  $\pm 12$  MHz as shown in Fig. 4(b), the dynamics remain similar from sweep to sweep.

The main characterisation technique used in swept source OCT is that of coherence roll-off. A coherence roll-off measurement is used to examine two main imaging properties of an OCT system. The first is to examine the loss of signal strength with imaging depth due to the finite coherence of the source. The second is to measure the axial point spread function. In order to accomplish this, a series of reflectivity measurements are made using a single reflecting surface at various depths. By imaging a single ideal impulse the point spread function can be determined, while the sensitivity roll-off is observed by repeating the measurement and incrementally moving the sample reflector. Typically, the coherence roll-off is reported as the  $-3$  dB signal fall-off depth. This depth will provide a similar metric as the coherence depth,  $z_c$ , defined above in (9).

In general, a roll-off measurement is formed from multiple separate axial scans, and therefore defines a multi-shot averaged measurement. Using the presented interferometric technique, it is



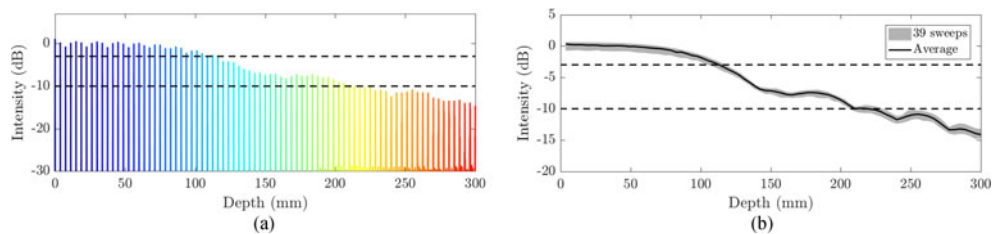


Fig. 6. (a) Single-shot roll-off in air calculated from the reconstructed electric field. The 3 dB sensitivity depth is approximately 100 mm. (b) Average roll-off envelope corresponding to 39 consecutive sweeps (black), along with the maximum and minimum peak values (grey area).

possible to numerically calculate the coherence roll-off using only a single sweep, even with many different scan depths. In this way, only a single sweep is used to define the roll-off, which can then be measured as a function of sweep number. Furthermore, previous roll-off measurements are determined by not only the laser source, but also the interferometer optics and detection set-up. With a numerically simulated roll-off, experimental errors can be limited, and it is easier to perform a direct comparison between the performance of different swept sources independent of the exact OCT apparatus employed. Again, the electric field reconstruction technique enhances the information that can be gained from the device under test.

The roll-off of the VCSEL is presented in Fig. 6(a). The roll-off is calculated by numerically delaying a copy of the laser electric field and mixing the signals. The signals are resampled to account for the internal k-clock and truncated to account for the laser start trigger discussed previously. The beat signal is Hanning windowed and the FFT computed for each value of the delay. Each of the images are then displayed together to observe the signal decay. The observed  $-3$  dB roll-off depth is approximately 100 mm, with a  $-10$  dB depth greater than 200 mm. These results are consistent with previously reported roll-off values for this type of laser [13], [28]. Fig. 6(b) displays the roll-off envelope, this time averaged across the 39 recorded sweeps. The grey area displays the maximum and minimum values, showing some intra-sweep variation in the envelope. The sweep-to-sweep variation in this value leads to a roll-off depth of  $95 \pm 5$  mm. Compared to the coherence imaging depth calculated earlier ( $z_c = 670$  mm), the roll-off estimate is more conservative. The difference between these two measurements stems from the slightly different definitions of the spectral width and temporal coherence employed in each case. The linewidth-based method is chosen in order to provide a more general method which does not assume a set lineshape or roll-off envelope shape. Generally, the coherence imaging depth tends to be between a factor of 5 and 7 times the roll-off depth, and this has been seen to be consistent for multiple swept sources.

Fig. 6(a) shows a series of peaks formed by imaging an ideal reflector using the electric field of a single sweep. The axial point spread function (PSF) associated with the laser will be the shape of these imaged peaks. The PSF stems from the windowing of the recorded beating signal, both due to the finite extent of the beat signal, as well as the intensity envelope during the sweep. The PSF is also widened by the presence of extra sweep nonlinearities, which chirp the beating signal. Of interest in the PSF is how its width changes with respect to the delay depth. Generally, the longer the delay between the fields, the larger the effect of sweep irregularities on the PSF. Fig. 7 presents the measured average PSF width as a function of the imaging depth. The PSF can be well approximated by a Gaussian, with a FWHM of less than  $10 \mu\text{m}$  at short imaging depths, as expected for a sweep with an optical bandwidth of 80 nm. The error bars of this figure indicate the standard deviation of the FWHM across 39 consecutive sweeps, showing a common degradation of the PSF with imaging depth by approximately  $3\text{--}4 \mu\text{m}$  over 120 mm imaging depth. The inset of Fig. 7 shows a single-shot PSF peak at a depth of 7.5 mm, along with the Gaussian fit indicating a FWHM of  $8.1 \mu\text{m}$ . This measurement offers previously unavailable insight into the achievable dynamic imaging performance of the tunable VCSEL OCT applications. As a whole, the  $3 \times 3$  characterisation technique that has been presented enables novel characterisation of

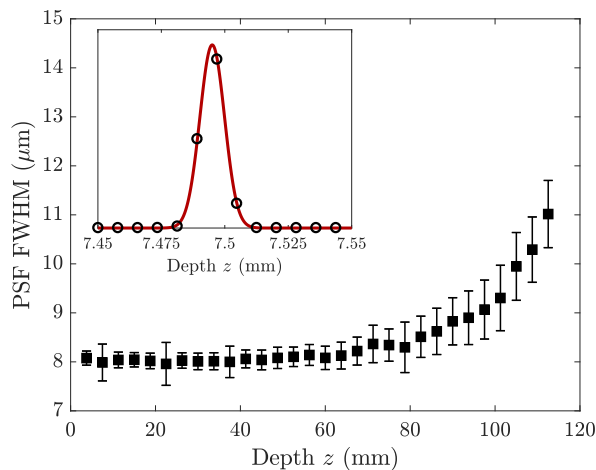


Fig. 7. Average PSF width in air across 39 consecutive sweeps, defined as the FWHM of a Gaussian fit to the peak, as a function of scan depth. (Inset) A single roll-off peak (circles) fitted with a Gaussian function (line). The point spread function width is determined to be  $8.1 \mu\text{m}$ .

real-time laser properties that can be invaluable in understanding the swept source, its strengths, and possible improvements for future swept light sources.

#### 4. Conclusion

This work provides an extensive look at the power of the self-delayed heterodyne method. A state of the art swept VCSEL is considered, which has a 200 kHz sweep rate and  $>100 \text{ nm}$  sweep width. Measurement of the average linewidth and spectral shape revealed that the linewidth is significantly lower than other swept sources, at 224 MHz. Such a low linewidth implies that the coherence length of the light is more than suitable for ultra-long OCT applications. In many modern OCT systems, the limit on the maximum imaging depth would actually stem from the finite sampling speed of the analogue to digital converter elements, and as such no coherence-related signal decay would be expected. The long coherence length finding is consistent with the computed laser roll-off, showing available imaging depths of at least 100 mm. Dynamic measurement of the linewidth reveals that the linewidth is lowest during the centre of the sweep, with some undesirable frequency noise present at the beginning of the imaging acquisition time. Finally, the PSF of the laser was measured in air showing that although the width of the peak increases with depth, it remains below  $10 \mu\text{m}$  during the main imaging region of 0–100 mm.

Complete characterisation of the dynamic state of a swept laser is the most comprehensive way of monitoring the performance of the laser in imaging applications. The presented interferometric metrology technique offers full characterisation of swept laser output in a single-shot, time-resolved manner. Recovery of the electric field allows measurement of both direct laser parameters such as instantaneous frequency, linewidth, and spectrum; while also providing a simple method to calculate other related laser benchmarks such as coherence roll-off and point spread function. Crucially, the  $3 \times 3$  technique offers two advantages over other methods. Firstly, the fibre based interferometric measurement allows the device under test to be examined free from any larger OCT apparatus, ensuring easy comparison between different swept source configurations and cavity geometries. By reconstructing the entire complex electric field of the laser, it becomes possible to directly compare the dynamics and imaging expectations in real-time while varying laser parameters. The other advantage of this technique is in the unparalleled access granted to both the inter-sweep and intra-sweep properties. Laser parameters can be tracked over subsequent sweeps and sweep to sweep changes, as well as laser evolution during the sweep, can be easily compared. This type

of full field characterisation is an excellent tool that could provide invaluable insight into the design and optimisation of next generation swept sources.

## Acknowledgment

P. M. McNamara, K. Neuhaus, and M. Leahy have a financial interest in Compact Imaging, Inc.

## References

- [1] J. Fujimoto and W. Drexler, "Introduction to optical coherence tomography," in *Opt. Coherence Tomography*, W. Drexler and J. Fujimoto, Eds. Berlin, Germany: Springer, 2008.
- [2] M. Wojtkowski, "High-speed optical coherence tomography: Basics and applications," *Appl. Opt.*, vol. 49, pp. D30–D69, 2010.
- [3] T. Klein, W. Wieser, C. Eigenwillig, B. Biedermann, and R. Huber, "Megahertz OCT for ultrawide-field retinal imaging with 1050 nm Fourier domain mode-locked laser," *Opt. Exp.*, vol. 19, pp. 3044–3062, 2011.
- [4] K. Imai, Y. Shimada, A. Sadr, Y. Sumi, and J. Tagami, "Noninvasive cross-sectional visualization of enamel cracks by optical coherence tomography in vitro," *J. Endodontics*, vol. 38, pp. 1269–1274, 2012.
- [5] J. Su, J. Zhang, L. Yu, H. Colt, M. Brenner, and Z. Chen, "Real-time swept source optical coherence tomography imaging of the human airway using a microelectromechanical system endoscope and digital signal processor," *J. Biomedical Opt.*, vol. 13, 2008, Art. no. 030506.
- [6] G. Tearney *et al.*, "Scanning single-mode fiber optic catheter-endoscope for optical coherence tomography," *Opt. Lett.*, vol. 21, pp. 543–545, 1996.
- [7] G. Song and K. Harding, "OCT for industrial applications," *Proc. SPIE*, vol. 8563, 2012, Art. no. 85620N.
- [8] M. Choma, M. Sarunic, C. Yang, and J. Izatt, "Sensitivity advantage of swept source and Fourier domain optical coherence tomography," *Opt. Exp.*, vol. 11, pp. 2183–2189, 2003.
- [9] R. Huber, M. Wojtkowski, and J. Fujimoto, "Fourier domain mode locking (FDML): A new laser operating regime and applications for optical coherence tomography," *Opt. Exp.*, vol. 14, pp. 3225–3237, 2006.
- [10] R. Huber, M. Wojtkowski, J. Fujimoto, J. Jiang, and A. Cable, "Three dimensional and C-mode OCT imaging with a compact, frequency swept laser source at 1300 nm," *Opt. Exp.*, vol. 13, pp. 10523–10538, 2005.
- [11] M. Bonesi *et al.*, "Akinetic all-semiconductor programmable swept-source at 1550 nm and 1310 nm with centimeters coherence length," *Opt. Exp.*, vol. 22, pp. 2632–2655, 2014.
- [12] M. Kuznetsov, W. Atia, B. Johnson, and D. Flanders, "Compact ultrafast reflective Fabry-Pérot tunable lasers for OCT imaging applications," *Proc. SPIE*, vol. 7554, 2010, Art. no. 75541F.
- [13] I. Grulkowski *et al.*, "Retinal, anterior segment and full eye imaging using ultrahigh speed swept source OCT with vertical-cavity surface emitting lasers," *Biomedical Opt. Exp.*, vol. 3, pp. 2733–2751, 2012.
- [14] I. Grulkowski *et al.*, "High-precision, high-accuracy ultralong-range swept-source optical coherence tomography using vertical cavity surface emitting laser light source," *Opt. Lett.*, vol. 38, pp. 673–675, 2013.
- [15] V. Jayaraman, G. Cole, M. Robertson, A. Uddin, and A. Cable, "High-sweep-rate 1310 nm MEMS-VCSEL with 150 nm continuous tuning range," *Electron. Lett.*, vol. 48, pp. 867–868, 2012.
- [16] V. Jayaraman, J. Jiang, B. Potsaid, G. Cole, J. Fujimoto, and A. Cable, "Design and performance of broadly tunable, narrow line-width, high repetition rate 1310nm VCSELs for swept source optical coherence tomography," *SPIE OPTO*, vol. 8276, 2012, Art. no. 82760D.
- [17] B. Biedermann, W. Wieser, C. Eigenwillig, T. Klein, and R. Huber, "Direct measurement of the instantaneous linewidth of rapidly wavelength-swept lasers," *Opt. Lett.*, vol. 35, pp. 3733–3735, 2010.
- [18] B. Biedermann, W. Wieser, C. Eigenwillig, T. Klein, and R. Huber, "Dispersion, coherence and noise of Fourier domain mode locked lasers," *Opt. Exp.*, vol. 17, pp. 9947–9961, 2009.
- [19] T. Butler *et al.*, "Single shot, time-resolved measurement of the coherence properties of OCT swept source lasers," *Opt. Lett.*, vol. 40, pp. 2277–2280, 2015.
- [20] Thorlabs, Inc., "MEMS-VCSEL Swept Source OCT," 2016. [Online]. Available: [http://www.thorlabs.de/newgrouppage9.cfm?objectgroup\\_id=6473](http://www.thorlabs.de/newgrouppage9.cfm?objectgroup_id=6473). Accessed on: Feb. 12, 2016.
- [21] D. Goulding, T. Butler, B. Kelleher, S. Slepneva, S. Hegarty, and G. Huyet, "Visualisation of the phase and intensity dynamics of semiconductor lasers via electric field reconstruction," in *Nonlinear Dynamics: Materials, Theory and Experiments*, M. Tlidi and M. Clerc, Eds. Berlin, Germany: Springer, 2016.
- [22] J. Izatt and M. Choma, "Theory of optical coherence tomography," in *Optical Coherence Tomography*, W. Drexler and J. Fujimoto, Eds. Berlin, Germany: Springer, 2008.
- [23] H. Halbritter, C. Sydlo, B. Kogel, F. Riemenschneider, H. Hartnagel, and P. Meissner, "Linewidth and chirp of MEMS-VCSELs," *IEEE Photon. Technol. Lett.*, vol. 18, no. 20, pp. 2180–2182, Oct. 2017.
- [24] S. Todor, B. Biedermann, W. Wieser, R. Huber, and C. Jiruaschek, "Instantaneous lineshape analysis of Fourier domain mode-locked lasers," *Opt. Exp.*, vol. 19, pp. 8802–8807, 2011.
- [25] T. Pfeiffer, W. Draxinger, W. Wieser, T. Klein, M. Petermann, and R. Huber, "Analysis of FDML laser with meter range coherence," *Proc. SPIE*, vol. 10053, 2017, Art. no. 100531T.
- [26] S. Song, J. Xu, and R. Wang, "Long-range and wide field of view optical coherence tomography for in vivo 3D imaging of large volume object based on akinetic programmable swept source," *Biomed. Opt. Exp.*, vol. 7, pp. 4734–4748, 2016.
- [27] Z. Wang *et al.*, "Cubic meter volume optical coherence tomography," *Optica*, vol. 3, pp. 1496–1503, 2016.
- [28] S. Moon and E. S. Choi, "VCSEL-based swept source for low-cost optical coherence tomography," *Biomed. Opt. Exp.*, vol. 8, pp. 1110–1121, 2017.